Supporting Information

Vaden et al. 10.1073/pnas.1013391108

SI Text

Particle Generation. Dioctyl phthalate (DOP) and dioctyl sebacate (DOS) particles were generated by atomization of the neat liquids and loaded into a 100-L Teflon bag filled with particle-free zero air. Secondary organic aerosol (SOA) was generated by introducing 200 ppb of α-pinene and ∼500 ppb of O_3 into a clean 100-L Teflon bag. Approximately 250 ppm of cyclohexane was separately introduced into the bag as an OH scavenger. The gas-phase α-pinene reacted with O_3, and the oxidized organic products formed SOA particles by homogeneous nucleation. The size distributions of SOA particles were monitored with a scanning mobility particle sizer. Sampling of pure SOA particles began once particles stopped growing, ∼1.5 h from the α-pinene injection.

Coated particles were generated by carrying out the SOA generation procedure in a Teflon bag that contained a small amount of DOP, DOS, pyrene, or a mixture of all three plus benzo[ghi] perylene. These bulk samples were placed in the bottom of the bag and allowed to sit in the zero-air environment of the bag to allow their vapors to reach equilibrium. Previous experience, confirmed by mass spectrometry in the current work, shows that under such conditions homogeneously nucleated SOA particles acquire an adsorbed coating of the organic compound.

Ambient particles were sampled in situ, dried using two diffusion driers, connected in series, filled with drierite, and their densities measured using SPLAT II and a differential mobility analyzer (DMA), as described elsewhere (1). The sulfate content is calculated assuming that the density of the organic fraction is 1.25 $g\,cm^{-3}$ (1) and a sulfate density of 1.77 $g\,cm^{-3}$.

Particle Analysis. Particles were size-selected with a DMA and neutralized with ^{85}Kr source. This sample of monodisperse particles was then passed at ∼0.3 Lpm through two charcoal denuders, constructed by filling standard diffusion driers (TSI Inc., Model 3062) with activated charcoal, connected in series, and kept at room temperature. Particles were then loaded and stored in the 7-L stainless steel homebuilt evaporation chamber that was purged with zero air partially and contained ∼1 L of activated charcoal at the bottom of the chamber. The fact that the particles are generated in a separate chamber and that gas-phase organics in the evaporation chamber were continuously removed by the activated charcoal eliminates the gas–wall repartitioning problem. Low particle number concentrations in the chamber (∼10–200 particles cm^{-3}) provide the means to follow kinetics of single-particle evaporation. Particle evaporation was measured by recording the vacuum aerodynamic diameters (d_{va}) and mass spectra of the size-selected particles using SPLAT II, our single-particle mass spectrometer (vide infra), at different times during the evaporation process. Particles were either sampled by SPLAT II directly from the DMA to measure d_{va} at $t = 0$ or passed through the two denuders into SPLAT II, in which case we compute the evaporation time using the flow rate to determine the average residence time in the evaporation system (2 min). Long-time-scale evaporation measurements were made by sampling particles locked in the evaporation chamber. For these long-time evaporation measurements, particles were sampled directly from the chamber under constant-pressure conditions. The schematic of experimental setup is shown in Fig. 1 of the main text.

SPLAT II. SPLAT II has been described in detail elsewhere (2, 3). Briefly, particles enter into the instrument through an aerodynamic lens inlet used to transport the particles from the ambient air into the vacuum system with extremely high efficiencies. The aerodynamic lens forms a low divergence particle beam and imparts on each particle a velocity that is a narrow function of the particle d_{va}. Individual particles are detected by light scattering at two optical detection stages located 10.5 cm apart. The particle time of flight (PTOF) between the two stages is used to calculate particle velocity and determine the d_{va} with 0.5% precision. The particle detection event and the PTOF are then used to generate triggers to fire the IR and UV lasers for particle evaporation and ionization, respectively. Individual particle chemical compositions are determined from the acquired mass spectra using an angular reflectron time-of-flight mass spectrometer. Particle density and shape are determined based on the measurements of d_{va} distribution of size-selected particles (3).

In the present work, particle evaporation is quantified by measuring changes in particle d_{va}, which is a function of particle size, shape, and density according to Eq. **S1**:

$$d_{va} = \rho \bullet d_p/\chi_v \bullet \rho_0, \qquad \textbf{[S1]}$$

where d_p is the particle diameter, χ_v is the particle dynamic shape factor in the free molecular regime, and ρ and ρ_0 are particle density and unit density, respectively.

The observed narrow line shape of the d_{va} size distribution for size-selected SOA particles indicates that SOA remain spherical throughout the entire evaporation process (3). We have measured the particle density as a function of evaporation time and found that at the early stages of evaporation particle density reproducibly increased by 2% and remained constant thereafter. Particle sphericity and the small change in density mean that changes in d_{va} are directly related to changes in particle size. The slight increase in particle density is consistent with a change in particle phase and/or composition.

Analysis of Pure DOP Evaporation. Fig. 2 shows that d^2/d_0^2 for DOP particles decrease nearly linearly as a function of time. Following the analysis presented in refs. 4 and 5, the slope of d^2/d_0^2 vs. time is related to the vapor pressure as

$$\text{slope} = \frac{-8\beta D_{ij} M_i p_j^0}{\rho RT}, \qquad \textbf{[S2]}$$

where β is a parameter that depends on the Knudsen number (here, taken as 0.1), D_{ij} is the diffusivity of vapor-phase DOP (component i) in air (medium j), M_i is the DOP molecular weight, p_j^0 is the vapor pressure, ρ is the particle density, R is the universal gas constant, and T is the temperature. Of these constants, only D_{ij} is not known exactly. We obtained the slope of the d^2/d_0^2 vs. time plot and used the DOP diffusivity from Ray et al. (6) to calculate the vapor pressure as 10^{-7} Torr. Slightly different vapor pressure values, within ∼15% of each other, were obtained for different particle sizes. These calculated DOP vapor pressures are in excellent agreement with previously reported values (7). DOP vapor pressures reported by Tang and Munkelwitz (7) for the range of our room temperatures of 23–24 °C are 9.5×10^{-8} and 1.13×10^{-7} Torr, respectively.

Experiments on DOS yielded similar results. Using known literature values for DOS density and molecular weight from the slope of d^2/d_0^2 vs. time, and the diffusivity of vapor-phase DOP we obtain vapor pressure of $1.95\cdot 10^{-8}$ Torr, which is in very good agreement with the reported value of $\sim 2\cdot 10^{-8}$ Torr for DOS at 25 °C (8).

Most importantly, the DOP and DOS examples validate the experimental methodology for investigating SOA evaporation kinetics.

Biexponential Fits of Experimental Data in Figs. 3–7. The biexponential functions given below for a number of SOA particle systems represent empirical fits to the experimental evaporation data and are plotted as lines in Figs. 3–7.

Pure SOA:

$$\left(\frac{d}{d_0}\right)^3 = 0.48 * e^{(-0.0285*t)} + 0.52 * e^{(-4.0\bullet 10^{-4}*t)}. \quad \textbf{[S3]}$$

Aged pure SOA:

$$\left(\frac{d}{d_0}\right)^3 = 0.42 * e^{(-0.0285*t)} + 0.58 * e^{(-4.0\bullet 10^{-4}*t)}. \quad \textbf{[S4]}$$

DOP/DOS SOA:

$$\left(\frac{d}{d_0}\right)^3 = 0.27 * e^{(-0.0285*t)} + 0.73 * e^{(-3.3\bullet 10^{-4}*t)}. \quad \textbf{[S5]}$$

Aged DOP/DOS SOA:

$$\left(\frac{d}{d_0}\right)^3 = 0.15 * e^{(-0.0285*t)} + 0.85 * e^{(-2.5\bullet 10^{-4}*t)}. \quad \textbf{[S6]}$$

Pyrene SOA:

$$\left(\frac{d}{d_0}\right)^3 = 0.18 * e^{(-0.0285*t)} + 0.82 * e^{(-4.35\bullet 10^{-5}*t)}. \quad \textbf{[S7]}$$

Aged pyrene SOA:

$$\left(\frac{d}{d_0}\right)^3 = 0.055 * e^{(-0.0285*t)} + 0.945 * e^{(-4.35\bullet 10^{-5}*t)}. \quad \textbf{[S8]}$$

Mixture SOA:

$$\left(\frac{d}{d_0}\right)^3 = 0.075 * e^{(-0.0285*t)} + 0.205 * e^{(-7.35\bullet 10^{-3}*t)} + 0.72 * e^{(-3.35\bullet 10^{-5}*t)}. \quad \textbf{[S9]}$$

Ambient SOA on June 26:

$$\left(\frac{d}{d_0}\right)^3 = 0.135 * e^{(-0.015*t)} + 0.865 * e^{(-2.0\bullet 10^{-4}*t)}. \quad \textbf{[S10]}$$

Ambient SOA types 43 and 44 June 25:

$$\left(\frac{d}{d_0}\right)^3 = 0.2 * e^{(-0.03*t)} + 0.8 * e^{(-2.0\bullet 10^{-4}*t)}. \quad \textbf{[S11]}$$

Ambient SOA type 43 June 26:

$$\left(\frac{d}{d_0}\right)^3 = 0.135 * e^{(-0.015*t)} + 0.865 * e^{(-2.0\bullet 10^{-4}*t)}. \quad \textbf{[S12]}$$

Ambient SOA type 44 June 26:

$$\left(\frac{d}{d_0}\right)^3 = 0.2 * e^{(-0.015*t)} + 0.8 * e^{(-2.0\bullet 10^{-4}*t)}. \quad \textbf{[S13]}$$

Ambient SOA types 43 and 44 June 27:

$$\left(\frac{d}{d_0}\right)^3 = 0.16 * e^{(-0.03*t)} + 0.84 * e^{(-2.0\bullet 10^{-4}*t)}. \quad \textbf{[S14]}$$

Ambient SOA June 28:

$$\left(\frac{d}{d_0}\right)^3 = 0.2 * e^{(-0.018*t)} + 0.8 * e^{(-2.0\bullet 10^{-4}*t)}. \quad \textbf{[S15]}$$

Modeling. The time-dependent evaporation of multicomponent SOA particles is modeled by solving mass transfer equations assuming that particles are suspended in a gas free of organics. We assume that concentrations of organics in the gas phase remains zero over the entire modeling period because the activated charcoal is removing them. The kinetic mass transfer equations are written only for the particle phase. The 7-bin volatility basis sets obtained by Pathak et al. (9) from fits to low NO_x dark ozonolysis of α-pinene SOA formation data are used to represent partitioning properties of α-pinene SOA mixture (9, 10).

The mass flux of compound i (representing a given volatility bin) from the droplet of size k is calculated using Eq. **S16**.

$$J_{i,k} = 2\Pi N_k d_k D_i f(Kn,a)(c_i - c_i^{eq}\eta), \quad \textbf{[S16]}$$

where $J_{i,k}$ is the flux of species i from aerosol of size k, N_k and d_k are the number and diameter of particle k, respectively, D_i, C_i, and C_i^{eq} are the diffusivity, bulk gas-phase concentration of species i away from the particle surface, and equilibrium concentration of species i at the particle surface, respectively, $f(Kn,a)$ is the correction for noncontinuum effects and imperfect accommodation, Kn is the Knudsen number, a is the accommodation coefficient, and η is the Kelvin effect correction. The equilibrium concentration of each species i C_i^{eq} is calculated assuming absorptive partitioning in pseudoideal solution:

$$c_i^{eq} = x_{i,k}c_i^*, \quad \textbf{[S17]}$$

where $X_{i,k}$ is the mass fraction of species i in the particle of size k, c_i^* is the effective saturation concentration of species i (equal to saturation concentration of corresponding to 7-bin volatility basis sets (VBSs) ranging from 0.01 to 10^4 $\mu g\,m^{-3}$). As discussed earlier, bulk gas-phase concentration C_i in Eq. **S16** is assumed to be zero for all organic species throughout the modeling period. In addition, because all the evaporation measurements were conducted at room temperature, enthalpy of vaporization—ΔH_{vap}—does not affect the calculations, reducing uncertainties commonly encountered when dealing with thermal desorption data.

The initial aerosol mass fractions of each lumped species i (corresponding to a volatility bin) are estimated from given α_i from the fits (9), and using 200 ppb of consumed α-pinene. For all species i molecular weights of 150 $g\,mol^{-1}$, density of 1,500 $kg\,m^{-3}$, diffusion coefficient D_i of 5×10^{-6} $m^2\,s^{-1}$, and surface tension of 0.05 $N\,m^{-1}$ are assumed following Riipinen et al. (10). Particle evaporation rates are calculated as the sum of evaporation rates of all species i as

$$\frac{dmk}{dt} = \sum_{i=1}^{n} -J_{i,k}, \quad \textbf{[S18]}$$

where dm_k/dt is the instantaneous rate of change of mass of particle k, and $n = 7$ for the 7-bin VBS.

For any given calculation, all particles are assumed to be of the same size. Because particles do not interact with each other, particle evaporation rate does not depend on the total number of particles N_k. The value of N_k is chosen to achieve precision in the calculations. The Fortran Livermore Solver for Ordinary Differential Equations is used to solve the mass transfer equations

and output instantaneous particle diameters for comparison with experimental data.

Analysis of Mass-Spectral Data. The mass spectroscopic data recorded by SPLAT II throughout the study provide valuable information about particle compositions and their changes with evaporation time. In this section we provide a few examples that illustrate the type of information that the mass spectra provide.

Fig. S1 illustrates the changes in mass-spectral intensities with evaporation time for pure and coated α-pinene SOA particles. The Y axis in Fig. S1 reflects, for each variable, the fractional change in intensity relative to the maximum intensity the variable reaches. It shows that for laboratory SOA particles the intensity at m/z ihigher than 202 slowly increases with evaporation time, which could be interpreted to indicate oligomer formation. The intensity of the DOP-characteristic peak at $m/z = 149$, in DOP-coated SOA particles, rapidly drops with evaporation time and then remains constant at 20% of the original value. The relative intensity of the pyrene (PY) parent ion peak at $m/z = 202$, in PY-coated SOA, decreases so slowly such that ~50% of it remains even after 25 h of evaporation. The comparison between PY and DOP suggests that there are differences in morphological distribution of the solid PY and liquid DOP in the coated SOA particles.

Fig. S2 shows the average mass spectra of two distinct types of ambient SOA particles mixed with sulfate that were observed on June 25, 26, and 27. The mass spectra are labeled type 44 and type 43 to denote which of these two mass-spectral peaks has higher intensity prior to particle evaporation. Both are dominated by oxygenated organics, have identical density, and are mixed with the same amount of sulfate (~12%). Type 43 particles contain in addition to oxygenated organics and sulfate a small amount of organic amines. Examination of changes in mass-spectral intensities of ambient SOA particles with evaporation shows relatively minor changes. The increase in intensity at higher m/z that we observed for laboratory SOA is not observed here, and at lower m/z the most prominent changes are in the intensities of peaks 44 and 73. The intensity of these peaks, for both particle types, decrease rapidly with evaporation and remain constant thereafter. Fig. S3 shows changes in $m/z = 44$ as a function of time. This trend in peak intensity most likely indicates that some of their intensity belongs to surface coatings.

1. Zelenyuk A, Imre D, Han JH, Oatis S (2008) Simultaneous measurements of individual ambient particle size, composition, effective density, and hygroscopicity. *Anal Chem* 80:1401–1407.
2. Zelenyuk A, Yang J, Choi E, Imre D (2009) SPLAT II: An aircraft compatible, ultra-sensitive, high precision instrument for in-situ characterization of the size and composition of fine and ultrafine particles. *Aerosol Sci Tech* 43:411– 424.
3. Zelenyuk A, Imre D (2009) Beyond single particle mass spectrometry: Multidimensional characterisation of individual aerosol particles. *Int Rev Phys Chem* 28:309–358.
4. Davis EJ, Ravindran P, Ray AK (1980) A review of theory and experiments on diffusion from submicroscopic particles. *Chem Eng Commun* 5:251–268.
5. Zhang S-H, Seinfeld JH, Flagan RC (1993) Determination of particle vapor pressures using the tandem differential mobility analyzer. *Aerosol Sci Tech* 19:3–14.
6. Ray AK, Lee J, Tilley HL (1988) Direct measurements of evaporation rates of single droplets at large Knudsen numbers. *Langmuir* 4:631–637.
7. Tang IN, Munkelwitz HR (1991) Determination of vapor pressure from droplet evaporation kinetics. *J Colloid Interf Sci* 141:109–118.
8. Rader DJ, Mcmurry PH, Smith S (1987) Evaporation rates of monodisperse organic aerosols in the 0.02-μm-diameter to 0.2-μm-diameter range. *Aerosol Sci Tech* 6:247–260.
9. Pathak RK, et al. (2007) Ozonolysis of alpha-pinene: Parameterization of secondary organic aerosol mass fraction. *Atmos Chem Phys* 7:3811–3821.
10. Riipinen I, Pierce JR, Donahue NM, Pandis SN (2010) Equilibration time scales of organic aerosol inside thermodenuders: Evaporation kinetics versus thermodynamics. *Atmos Environ* 44:597–607.

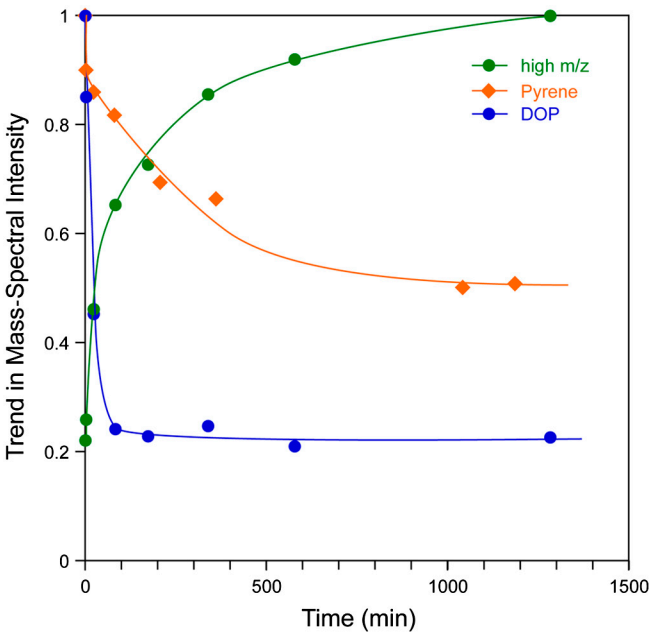

Fig. S1. Trends in mass-spectral intensities of high m/z for pure SOA and of DOP and PY characteristic peaks, as a function of evaporation times. See text for the details.

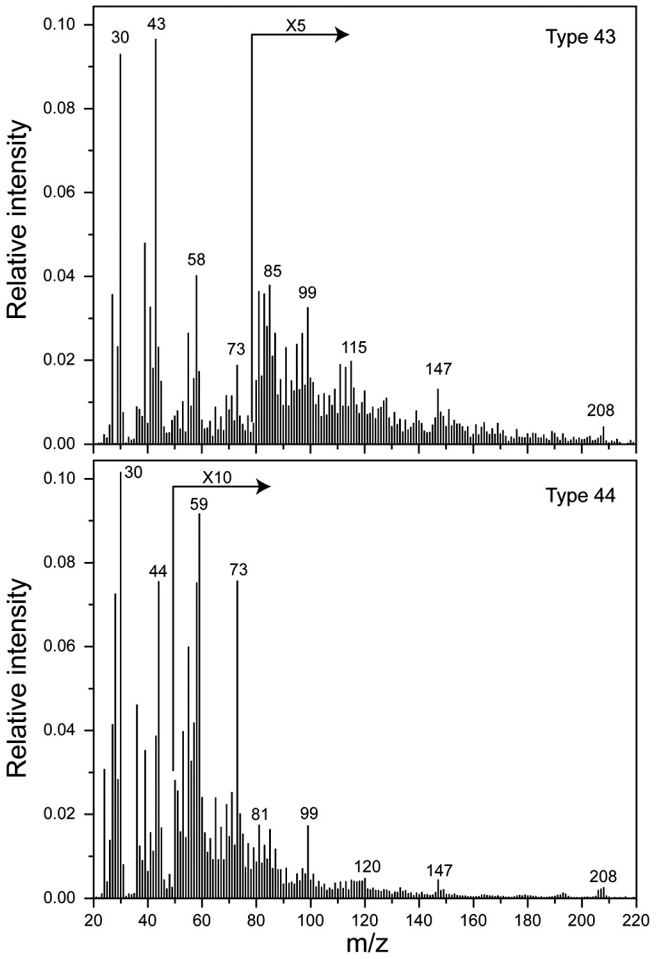

Fig. S2. Mass spectra of the two types of ambient SOA particles classified as type 43 and type 44.

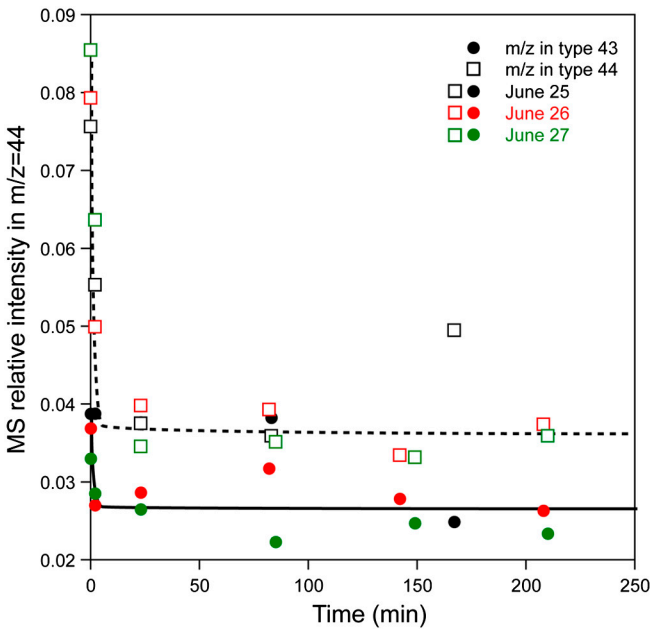

Fig. S3. Trends in the mass-spectral intensity of the peak at m/z = 44 for the two particle types.